journal

J. Am. Ceram. Soc., 76 [3] 729–36 (1993)

Cracking due to Localized Hot Shock

Viggo Tvergaard

Technical University of Denmark, Lyngby, Denmark

Z. Cedric Xia and John W. Hutchinson*

Harvard University, Cambridge, Massachusetts 02138

Results are presented for the cracking to be expected when a sudden temperature increase is applied over a localized region on a surface of a brittle solid. A localized temperature increase is applied to the surface of a body whose interior is initially at uniform temperature. A three-part analysis is conducted: (i) for the evolving temperature distribution, (ii) for the evolving thermal stresses induced by the nonuniform temperature field, and (iii) for stress intensity factors of cracks oriented either parallel to or perpendicular to the surface and initiated at times when the stresses are critical. Plane-strain and axisymmetric versions of the problems are considered. For the plane-strain problem, the complete trajectory of the crack is determined under the assumption that its tip advances maintaining a pure mode I field at all times. Conditions for excluding cracking due to localized hot shock are given.

I. Introduction

THE problem addressed is the susceptibility to cracking of a brittle solid subject to localized heating at a spot on its surface. An example of current concern is spalling due to hot shock in the coating process of ceramic fibers where molten droplets of coating material impinge the fiber, as discussed by Backman.[1] Figure 1 shows the hot shock damage on sapphire fiber which has been coated by a titanium matrix material deposited as molten droplets. The matrix material was subsequently removed, revealing the spall damage. Another example is when the localized heating of a surface of a brittle material irradiated by a laser beam produces a hemispherically shaped spall chip. Generally speaking, localized heating of a surface induces compressive stresses parallel to the surface near the surface, and thus it is not intuitively apparent how cracking occurs in hot shock. By investigating the stresses induced in a semi-infinite half-space subject to a suddenly imposed localized temperature increase, one finds that tensile stresses do occur in regions below the surface and in some cases even at the surface outside the heated region. In this paper, both one-dimensional and axisymmetric temperature increase distributions are considered, as depicted in Fig. 2. These are suddenly imposed and subsequently held constant. The resulting temperature distributions are obtained as a function of time, as are the stresses induced by the nonuniform thermal expansion. The time and place where a particular component of stress reaches its maximum tensile value are identified, and cracking initiated at this critical time is analyzed in some detail. This study does not deal with the coupled problem wherein a splat in contact with the substrate transfers its heat and consequently undergoes a change in temperature itself. The purpose of this paper is to gain insight into how cracking can arise in the simplest instances of localized hot shock. Subsequent work accounting for coupling and other effects, such as spalling due to bonding and subsequent cooling of the splat, will be necessary to refine the quantitative predictions arrived at here.

As a model to gain insight into the fiber spalling problem, Russell[2] has analyzed the effect of the sudden imposition of a uniform temperature increase ΔT_0 on the surface of a cylindrical body of radius R, i.e., the problem of an infinite solid cylinder suddenly thrust into a hot bath. Material at the surface of the cylinder experiences compressive stresses parallel to the surface, but the interior region near the axis of symmetry develops tensile stresses. The axial component of stress at the axis attains the largest tensile value, which is given by

$$\sigma_{zz}(1 - \nu)/(\alpha E \Delta T_0) \cong 0.47 \qquad (\nu = 0.3) \tag{1}$$

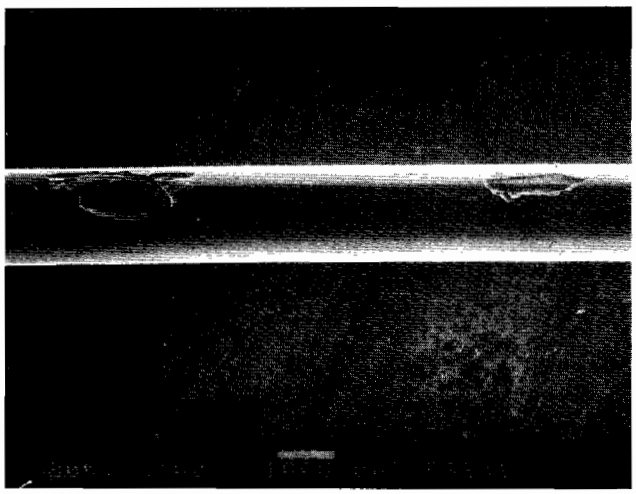

Fig. 1. Hot shock damage on a sapphire fiber (photograph supplied by E. S. Russell of GE Corp.).

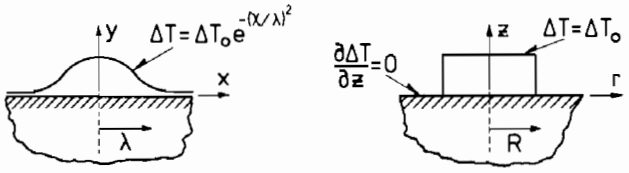

Fig. 2. Surface temperature distributions considered in this paper which are suddenly applied and subsequently held constant.

M. D. Thouless—contributing editor

Manuscript No. 195956. Received February 20, 1992; approved October 8, 1992.

The work of JWH and ZCX was supported in part by the DARPA University Research Initiative (Subagreement P.O. VB38639-0 with the University of California, Santa Barbara, ONR Prime Contract N00014-86-K0753) and the Division of Applied Sciences, Harvard University.

*Member, American Ceramic Society.

where E is Young's modulus, ν is Poisson's ratio, and α is the coefficient of thermal expansion. This value occurs after a time lapse from the imposition of ΔT_0 of

$$t \cong 0.075R^2/D \tag{2}$$

where D is the thermal diffusivity ($D = k/(\rho c_p)$, where k is the thermal conductivity, ρ is the mass density, and c_p is the specific heat). Thus, if a critical stress σ_c for initiating a crack is invoked, the model predicts that no crack will be initiated if

$$\Delta T_0 < 2.13(1 - \nu)\sigma_c/(\alpha E) \tag{3}$$

Russell[2] also considers the influence of barriers to perfect thermal conductivity at the fiber surface and their role in lowering the peak tensile stress.

II. Hot Shock in Plane Strain

An infinite half-space lying below the x-axis has uniform E, ν, α, and D. At $t = 0$ it has a uniform temperature, and at that instant a temperature increase

$$\Delta T = \Delta T_0 e^{-(x/\lambda)^2} \qquad (\text{on } y = 0) \tag{4}$$

is suddenly imposed on the traction-free upper surface and is subsequently maintained for all time. As sketched in Fig. 2(a), λ is the approximate half-width of the localized hot spot. A three-part problem is solved: (i) the temperature distribution in the half-space for $t > 0$, (ii) the stress distribution in the half-space for $t > 0$ which is induced by the nonuniform temperature field, and (iii) two cracking problems associated with cracks initiated at flaws located at the points where the maximum tensile stress components occur.

(1) Temperature Distribution

The change of temperature in the interior of the half-space, $\Delta T(x,y,t)$, satisfies

$$\nabla^2(\Delta T) = D^{-1}\frac{\partial \Delta T}{\partial t} \tag{5}$$

subject to the initial conditions and Eq. (4) along with the condition that $\Delta T \to 0$ as $x^2 + y^2 \to \infty$. This is a classical problem which can be solved with the aid of transform methods. The solution is

$$\Delta T(x,y,t) = \Delta T_0 \frac{(-y)}{\pi}\int_{-\infty}^{\infty} \frac{e^{-(\eta/\lambda)^2}}{[(x-\eta)^2 + y^2]} \exp\left[-\frac{(x-\eta)^2 + y^2}{4Dt}\right] d\eta \tag{6}$$

(2) Stress Distribution

Under the assumption of plane strain conditions, the Airy stress function $\Phi(x,y)$ at a given instant t satisfies

$$\nabla^4\Phi = -[E\alpha/(1 - \nu)]\nabla^2(\Delta T) \tag{7}$$

where the in-plane stress components are given by $\sigma_{xx} = \Phi_{,yy}$, $\sigma_{yy} = \Phi_{,xx}$, and $\sigma_{xy} = -\Phi_{,xy}$. This equation is supplemented by traction-free conditions on $y = 0$, along with the requirement that the stresses vanish far from the hot spot. This problem, or others similar to it, have also appeared in the literature,[3,4] and neither the solution details nor the solution itself will be presented here. Closed-form expressions for the stress components $\sigma_{\alpha\beta}(x,y,t)$ are obtained which involve double integration over the half-space. These integrals are evaluated numerically to obtain the stress at any point at any time.

Plots of the two normal components directly beneath the center of the hot spot on $x = 0$ are shown in Fig. 3 for various values of the nondimensional time variable, tD/λ^2. The maximum tensile value of $\sigma_{xx}(0,y,t)$ is given by the following and occurs at the position and time given by

$$\frac{(1-\nu)\sigma^*_{xx}}{\alpha E \Delta T_0} = 0.0951 \quad \frac{y^*}{\lambda} = -0.505 \quad \frac{t^*D}{\lambda^2} = 0.023 \tag{8}$$

The maximum tensile value of $\sigma_{yy}(0,y,t)$ and associated location and time are given by

$$\frac{(1-\nu)\sigma^*_{yy}}{\alpha E \Delta T_0} = 0.0438 \quad \frac{y^*}{\lambda} = -1.23 \quad \frac{t^*D}{\lambda^2} = 0.098 \tag{9}$$

A feature of the plane-strain hot-shock problem which follows immediately from Eq. (7) is that the in-plane stresses approach zero as the temperature distribution approaches steady state (i.e., as $\nabla^2(\Delta T) \to 0$ as $t \to \infty$). This trend is reflected in the plots of Fig. 3.

(3) Crack Trajectories and Stress Intensity Factors

At the time t^*, corresponding to either Eq. (8) or Eq. (9), a very short crack of length $a_1 + a_2$ is introduced at the point $(0,y^*)$ where the maximum tensile stress occurs. For Eq. (8), the initiating crack is taken parallel to the y-axis, while for Eq. (9) it is taken parallel to the x-axis. Given the stress distribution at fixed time t^*, the crack trajectory is determined under the condition that the advancing tip is always in a state of pure mode I.

First, consider a crack initiated parallel to the y-axis at $(0,y^*)$ with the stress distribution associated with t^*, as pictured in the insert of Fig. 4(a). Symmetry dictates that a crack extending along the y-axis will have mode I conditions at its crack tip. For

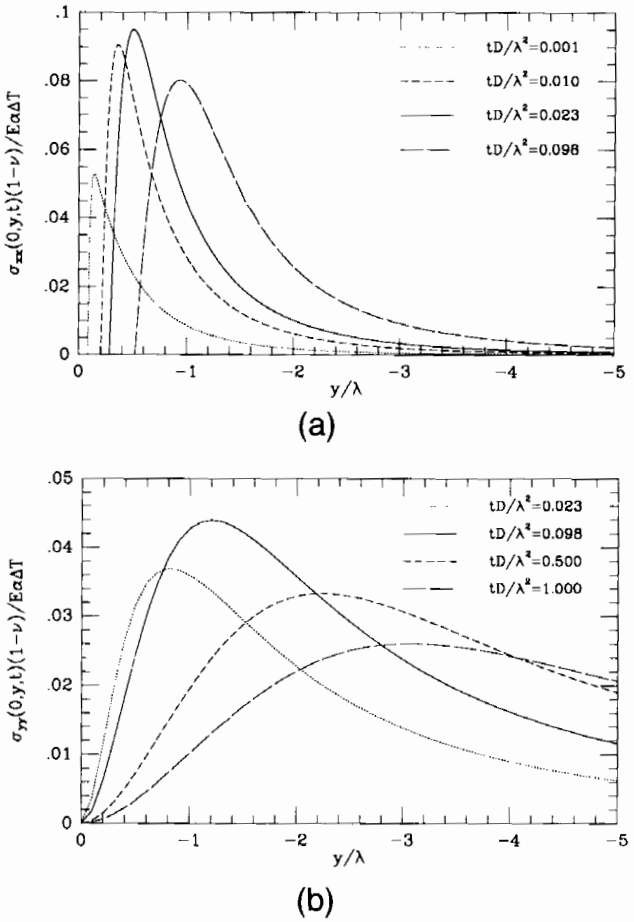

Fig. 3. Stress distributions directly below the hottest point on the surface for the plane strain problem.

a sufficiently small crack length compared to y^*, the mode I intensity factor at each tip is given by

$$K_I \cong \sigma_{xx}^* \sqrt{\pi(a_1 + a_2)/2} \tag{10}$$

Plots of K_I at the top and bottom crack tips are given in Fig. 4. The solution method for determining K_I is discussed in the Appendix. The stress intensity factor of the upper tip increases as the crack length initially increases but then goes to zero as the tip approaches the free surface, advancing into the region where σ_{xx} is compressive. As the lower tip dives deeper into the half-space, the stress intensity factor also decreases after first increasing. Given the toughness of the material, K_{Ic}, one can determine arrest lengths, a_1 and a_2, from the information in Fig. 4. If σ_c is the critical stress associated with some initial flaw size, then, by Eq. (8), cracks parallel to the y-axis will not be initiated if

$$\Delta T_0 < 10.5(1 - \nu)\sigma_c/(\alpha E) \tag{11}$$

Now, consider cracks initiated parallel to the x-axis at $(0,y^*)$ at time t^* given by Eq. (9). A very short crack extending from $(-a,y^*)$ to (a,y^*) will be in mode I at each tip with

$$K_I \cong \sigma_{yy}^* \sqrt{\pi a} \tag{12}$$

If it were to extend as a straight crack, it would develop a mode II stress intensity factor in addition to mode I. Curved trajectories for the crack extending symmetrically about its midpoint have been computed under the criterion that pure mode I conditions exist at all times at its tips. The calculations are therefore for a crack of increasing length (with symmetry enforced with respect to $x = 0$) advancing with a curved trajectory determined incrementally such that $K_{II} = 0$ is always in effect. The calculation, which is dicussed further in the Appendix, is started with a very short, straight crack. The stresses in the uncracked half-space as determined in Section II(2) is $\sigma_{\alpha\beta}(x,y,t^*)$, and this distribution is used in carrying out the calculations for the subsequent development of the cracks. Calculations of crack trajectories based on the criterion of pure mode I growth have been carried out in other contexts by Wawrzynek and Ingraffea,[5] Swenson and Kaushik,[6] Fleck,[7] and Freund and Kim.[8]

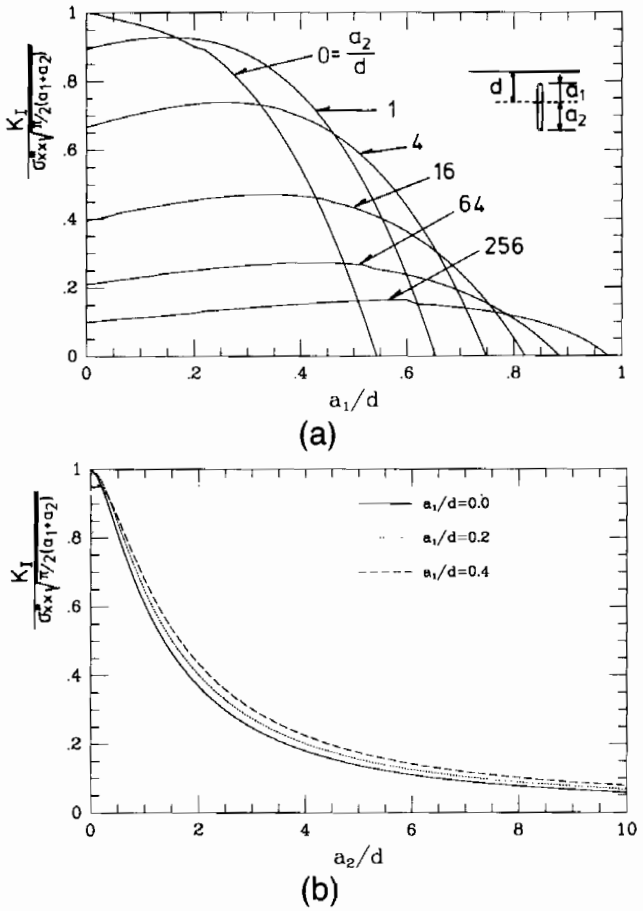

Fig. 4. Stress intensity factor in plane-strain problem for (a) upper tip and (b) lower tip. In each figure σ_{xx}^* is given by Eq. (8) and $d = -y^* = 0.505\lambda$.

Three crack trajectories are shown in Fig. 5(a). The curve labeled A is initiated at $(0,y^*)$, and those labeled B and C are initiated above and below $(0,y^*)$, respectively, as can be seen from where each trajectory crosses the y-axis. There clearly is a tendency for the cracks to seek out a depth roughly equal to $y^* = -1.23\lambda$ and then propagate parallel to the interface. The mode I stress intensity factor is shown with different normalizations in Figs. 5(b) and 5(c), where it is plotted against the horizontal coordinate of the right tip and *not* against the half-length of the curved trajectory. From Fig. 5(b) it is noted that the result (Eq. (12)) for the short crack remains a good approximation for cracks with half-widths up to λ or larger. From Fig. 5(c), it is seen that the peak value of K_I occurs at a half-width of about 1.4λ with

$$K_I \cong \sigma_{yy}^* \sqrt{\pi\lambda} = 0.078\alpha E \Delta T_0 \sqrt{\lambda}/(1 - \nu) \tag{13}$$

For crack half-widths greater than 1.4λ, K_I falls slowly and has decreased only to about one-half of the peak value for a half-width of 5λ. Thus, the plane-strain model suggests that fairly extensive subsurface cracking, more or less parallel to the free surface, is possible if the temperature is high enough to initiate growth. With σ_c as the critical stress for initiation, Eq. (9) implies that these cracks will not be initiated if

$$\Delta T_0 < 22.8(1 - \nu)\sigma_c/(\alpha E) \tag{14}$$

Alternatively, since the peak value of K_I is given by Eq. (13), no crack parallel to the free surface, irrespective of size, can propagate if $(K_I)_{peak} < K_{Ic}$ or, equivalently,

$$\Delta T_0 < 12.9(1 - \nu)K_{Ic}/(\alpha E \sqrt{\lambda}) \tag{15}$$

III. Axisymmetric Hot Shock

The axisymmetric problem shown in Fig. 2(b) has somewhat different boundary conditions than the plane-strain problem just considered. The half-space has uniform temperature prior to the sudden imposition of an axisymmetric temperature increase, $\Delta T(r,0,t) = \Delta T_0$, for $t \geq 0$ on the free surface for $r < R$. For $r > R$, the free surface is taken to be perfectly insulated with $\partial(\Delta T)/\partial z = 0$ on $z = 0$. The three-part problem solved for the two-dimensional model is solved here. In the axisymmetric problem, however, a finite element method is used to solve each of the three parts. Discussion of some of the details of the computational procedures is given in the Appendix.

(1) Temperature Distribution

Contours of constant temperature at three times within the range of interest are shown in Fig. 6. These contours display the progression of the heated region as it expands downward into the half-space. The three times are $t = t_0$, $t = 2t_0$, and $t = 4t_0$ where $t_0 = 0.016R^2/D$.

(2) Stress Distribution

Contours of constant values of the two stress components, $\sigma_{\theta\theta}$ and σ_{zz}, are shown in Figs. 7 and 8, respectively, at the same three times. The maximum tensile value of $\sigma_{\theta\theta}$, the location on the axis of symmetry where it occurs, and the time it is attained are

$$\frac{(1 - \nu)\sigma_{\theta\theta}^*}{\alpha E \Delta T_0} = 0.085 \quad \frac{z^*}{R} \cong -0.46 \quad \frac{t^* D}{R^2} \cong 0.016 \tag{16}$$

These calculations were carried out using the value of Poisson's ratio, $\nu = 0.23$, and the quantities shown do have some dependence on ν. Nevertheless, the above combination including the

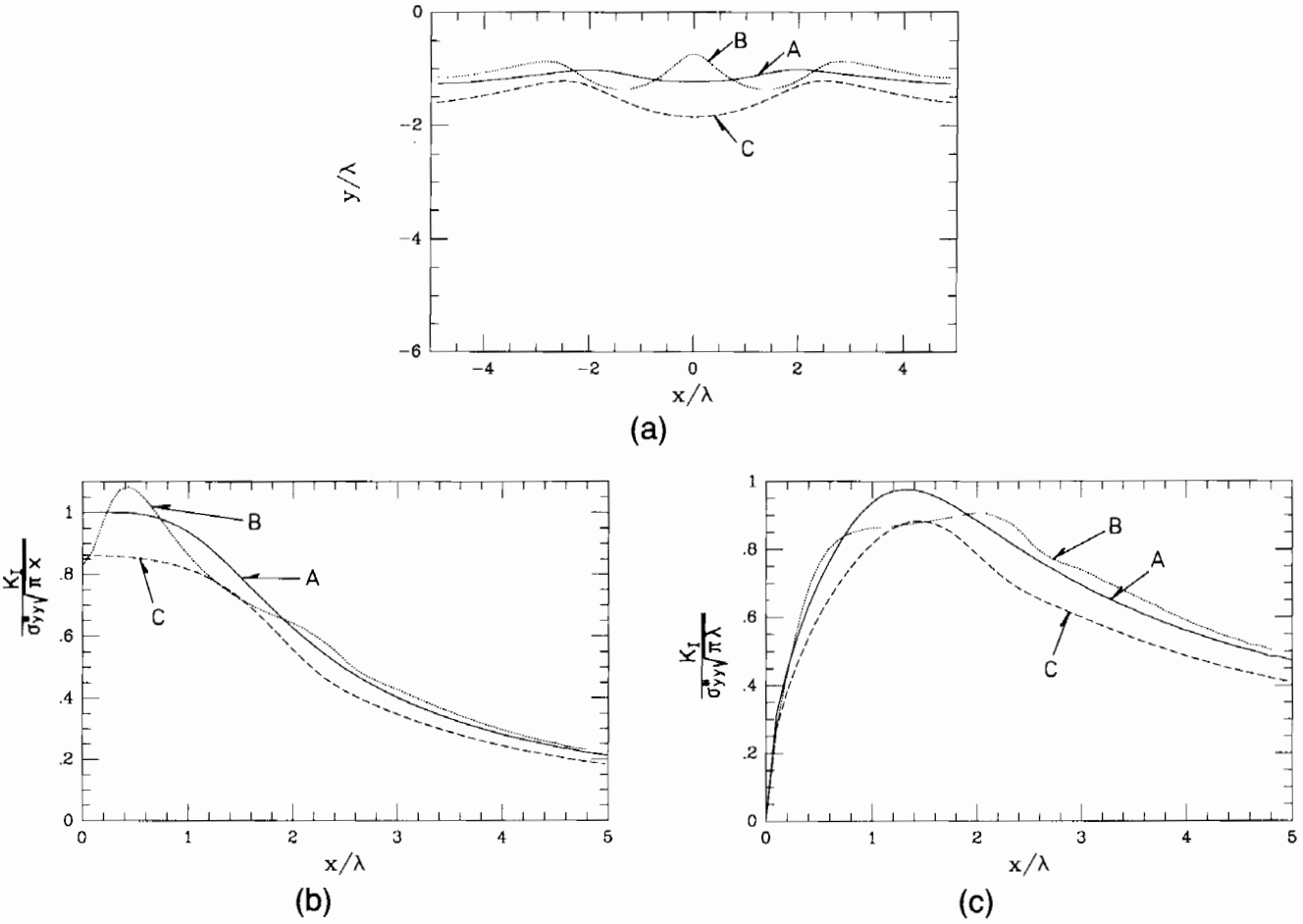

Fig. 5. (a) Mode I crack trajectories in the plane-strain problem. (b) and (c) Normalized stress intensity factor for crack in (a).

factor $(1 - \nu)$ does capture the approximate ν-dependence. This was established by repeating a few selected calculations with other values of ν. The circumferential component of stress also attains tensile values at the surface of the half-space outside the circular heated region, as can be seen in Fig. 7. The maximum tensile value of the circumferential stress at the surface, its position, and time of occurrence are approximately

$$\frac{(1-\nu)\sigma^*_{\theta\theta}}{\alpha E \Delta T_0} = 0.035 \quad \frac{r^*}{R} \cong 1.63 \quad \frac{t^* D}{R^2} \cong 0.064 \tag{17}$$

The maximum tensile value of σ_{zz} occurs along the axis of symmetry, and its value, position, and time of occurrence are

$$\frac{(1-\nu)\sigma^*_{zz}}{\alpha E \Delta T_0} = 0.070 \quad \frac{z^*}{R} \cong -0.95 \quad \frac{t^* D}{R^2} \cong 0.064 \tag{18}$$

The similarities between the tensile stresses in the axisymmetric and plane-strain problems are striking as can be seen by comparing Eq. (16) with (8) and Eq. (18) with (9). Of course, Eq. (17) has no analogue in plane strain. The maximum tensile stresses which occur in localized hot shock are about one order of magnitude smaller than the maximum compressive stress induced at the surface, which is $\alpha E \Delta T/(1 - \nu)$. In the axisymmetric problem, the peak tensile value of $\sigma_{\theta\theta}$ is slightly larger than the peak value of σ_{zz} and is attained earlier. Both the radial cracks aligned perpendicular to the surface and the spalling

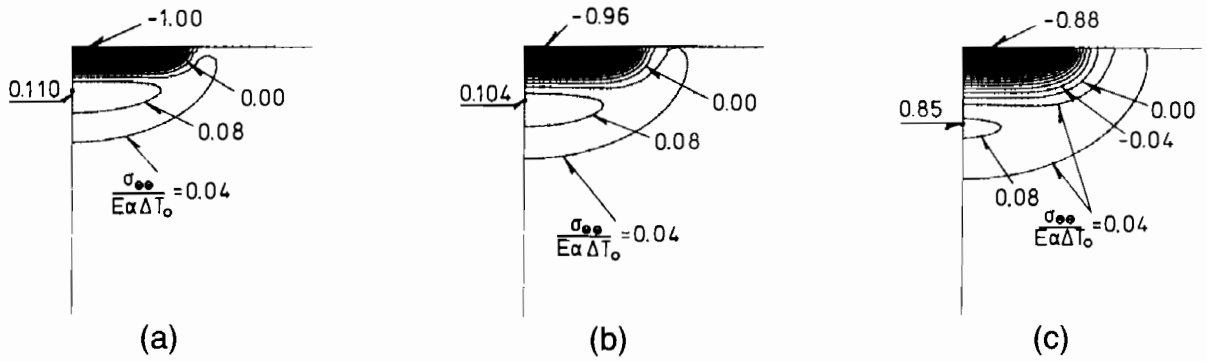

Fig. 6. Temperature distributions for the axisymmetric problem at (a) $t = t_0 = 0.016R^2/D$, (b) $t = 2t_0$, and (c) $t = 4t_0$.

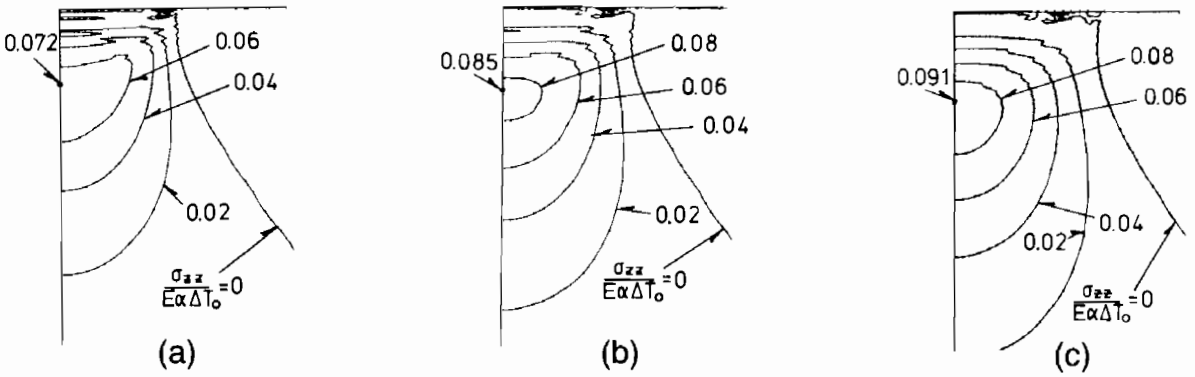

Fig. 7. Distributions of σ_{zz} in the axisymmetric problem at (a) $t = t_0$, (b) $t = 2t_0$, and (c) $t = 4t_0$.

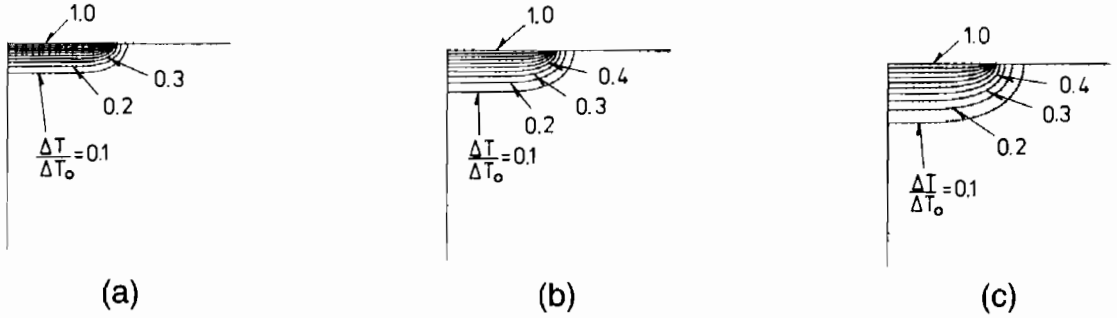

Fig. 8. Distributions of $\sigma_{\theta\theta}$ in the axisymmetric problem at (a) $t = t_0$, (b) $t = 2t_0$, and (c) $t = 4t_0$.

cracks aligned parallel to the surface can be produced by localized axisymmetric hot shock, although the radial cracks may be more prevalent than the spalling cracks for the reasons just mentioned. Both are most likely to be nucleated below the hot spot by subsurface flaws. The distribution of the circumferential stress is such that we can conjecture that a radial crack nucleated below the hot spot would arrest in the form of a crescent, which, if it reached the surface, would intersect the surface as a relatively short segment of radial crack lying just outside the perimeter of the hot spot.

A spalling crack nucleated parallel to the surface in the vicinity of the peak tensile value of σ_{zz} will spread outward as a penny-shaped crack, curving in response to the nonuniform stress distribution. No attempt has been made to compute the surface trajectories of pure mode I advance for the axisymmetric problem. Instead, calculations have been performed to determine the energy release rate and the mode I and mode II intensity factors for flat penny-shaped cracks spreading from small cracks centered at the axis of symmetry at a selection of depths and times. As in the plane-strain problem, it is found that cracks spreading from the point of maximum tensile stress will tend to spread more or less in a plane parallel to the surface.

(3) Stress Intensity Factors for Penny-Shaped Cracks Parallel to the Surface

Let σ_{zz}^* be the maximum tensile stress given by Eq. (18) at time t^*. A sufficiently small penny-shaped crack of radius a, aligned parallel to the surface and located on the axis at $z = z^*$, will be in mode I with

$$K_I \cong \frac{2}{\pi}\sigma_{zz}^*\sqrt{\pi a} = 0.079\alpha E\Delta T_0\sqrt{a}/(1-\nu) \tag{19}$$

The energy release rate is given by

$$G = \frac{(1-\nu^2)K_I^2}{E} = 0.0063\left(\frac{1+\nu}{1-\nu}\right)(\alpha\Delta T_0)^2 Ea \tag{20}$$

This result, which represents the maximum possible energy release rate for very short cracks, is shown in Fig. 9.

As the radius of the flat penny-shaped crack extends away from the axis, a mode II component of stress intensity will develop. Calculations have been carried out for a number of cases for flat penny-shaped cracks centered at various points along the axis of symmetry and subject to the stress field existing in the half-space at various times. Curves for the energy release rate,

$$G = \frac{(1-\nu^2)}{E}(K_I^2 + K_{II}^2) \tag{21}$$

normalized by $[(1+\nu)/(1-\nu)]ER(\alpha\Delta T_0)^2$, as a function of a/R are shown in Fig. 9. The curves are labeled by the depth, d, below the surface where the crack lies and the nondimensional time characterizing the stress distribution. The results in Fig. 9 were calculated with $\nu = 0.23$, but several calculations

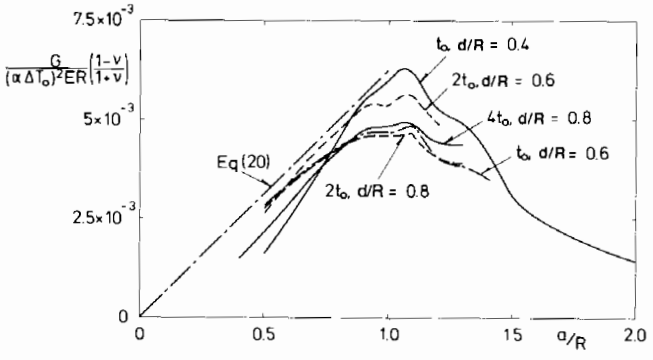

Fig. 9. Normalized energy release rate for penny-shaped cracks oriented parallel to the surface at a depth d below the surface and advancing into the stress distribution of the uncracked body associated with the times indicated.

repeated with $\nu = 0.4$ suggest that the normalization captures the Poisson's ratio dependence to a very good approximation. It can be noted from the results in Fig. 9 that the short crack limit (Eq. (20)) provides an excellent approximation for cracks with radii as large as the radius R of the heated spot. The companion curves giving the relative amount of mode II to mode I are plotted in Fig. 9, where the measure of mode mixity is taken as

$$\psi = \tan^{-1}(K_{II}/K_I) \tag{22}$$

Over the range of a/R for which calculations have been made, the mode II component of the stress intensity is relatively small compared to the mode I component. The general trend noted with respect to the trajectories in the plane-strain problem can be expected for the axisymmetric problem. Namely, when the crack is initiated at a depth which places it above the maximum of σ_{zz} on the axis, it will head downward but then begin to head upward again after it has reached a radius on the order of R. The present calculations do not allow one to conclude that the cracks will more or less parallel the surface at radii well in excess of R, as is the case in the plane-strain problem, but over the range of a/R considered there is no suggestion of any strong tendency for the crack to curve upward.

The maximum value of G over all the cases considered is

$$G = 0.0063\left(\frac{1+\nu}{1-\nu}\right)(\alpha\Delta T_0)^2 ER \tag{23}$$

occurring for the case $t = t_0$ with a crack depth of $d = 0.4R$ at a crack radius of $a \cong R$. From Fig. 10 it is seen that the crack is nearly mode I at this point, and thus the associated value of K_I is

$$K_I = 0.079\alpha E\Delta T_0\sqrt{R}/(1-\nu) \tag{24}$$

This result is remarkably close to the plane-strain result (Eq. (13)) when the effective half-width of the hot spot in plane strain is identified with the radius of the axisymmetric hot spot. Thus, it follows that the condition (Eq. (15)) for excluding cracking applies to axisymmetric cracking parallel to the surface as well if λ is exchanged with R.

To complete the results for the penny-shaped cracks, we have displayed the variations of the normalized energy release rate and ψ as a function of depth below the surface in Figs. 11 and 12, in each instance for $a/R = 1$. These variations are in accord with the previous discussion. In particular, it is noted that the largest energy release rates at finite crack radius (i.e., $a = R$) occur for cracks nucleated at times well before t^* associated with the peak tensile value of σ_{zz}^* in Eq. (18) and at a depth which is only about one-half of the critical depth for the smallest cracks.

IV. Discussion

When a temperature increase is suddenly imposed on the surface of a body at uniform temperature, the stress just below the hot spot is compressive with magnitude $\alpha E\Delta T_0/(1-\nu)$. Tensile stresses develop below the surface as the temperature increase diffuses into the solid. The magnitude of the largest tensile stresses documented in this work are not more that about one-tenth of the magnitude of the above maximum compressive stress. These tensile stresses develop on planes which are parallel to the surface and also on planes which are perpendicular to the surface. They occur at depths which are between one-half and one times the half-width or radius of the hot spot. In the case of the axisymmetric hot spot, circumferential tensile stresses develop at the surface outside the perimeter of the hot spot, but these stresses are only about one-half as large as the maximum subsurface tensile stresses.

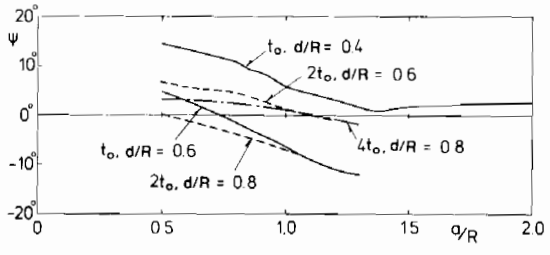

Fig. 10. Measure of mode mixity for cracks whose energy release rates are shown in Fig. 9.

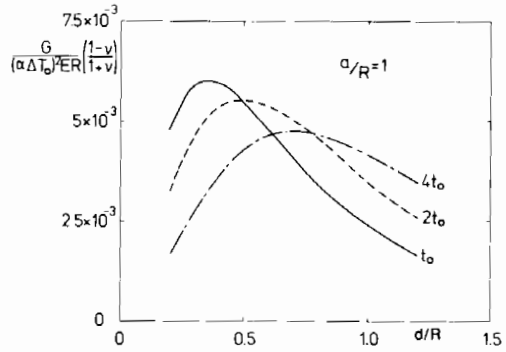

Fig. 11. Normalized energy release rate for penny-shaped cracks at various depths d, all with $a = R$, and advancing into the stress distribution of the uncracked body associated with the times indicated.

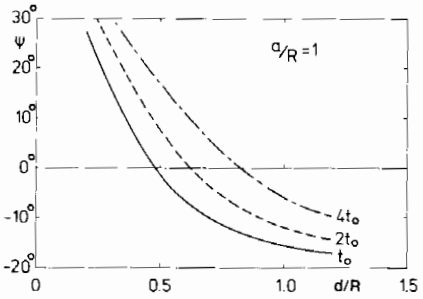

Fig. 12. Measure of mode mixity for cracks whose energy release rates are shown in Fig. 11.

The crack analyses indicate that subsurface cracks initiated parallel to the surface will tend to spread more or less parallel to the surface, and not necessarily curve up to the surface to generate a spall chip. Cracks initiated under the hot spot on planes perpendicular to the surface will remain in their plane and extend both upward and downward, and they also will not necessarily break through to the surface. In other words, the analyses suggest that hot shock may in some instances create subsurface damage which cannot be observed on the surface. There are several mechanisms not discussed here by which the cracks can travel to the surface and create a spall. If the radius of a crack running parallel to the surface becomes large enough relative to its depth below the surface, the compressive stress parallel to the surface can cause the platelike region above the crack to buckle away from the substrate. This, in turn, will induce mixed-mode conditions at the crack tip which will drive the tip to the surface as discussed in Ref. 9. Another possibility, noted in some model experiments (private communication by Eric Matthys, University of California, Santa Barbara), has not been discussed, where a splat solidifies and bonds to the substrate and then cools and contracts at a faster rate than the substrate, due to its higher coefficient of thermal expansion. This gives rise to a stress distribution somewhat akin to cold shock, which may be analyzed along the lines discussed in Section V. E of the article by Hutchinson and Suo.[9]

Matthys impinged molten drops of Ni at 1600°C on a quartz substrate. Using accoustic measurements, he observed two distinct cracking events: the first about 2 s after the droplet hit, which appeared to be entirely subsurface, and the second about 30 s later, involving spalling of the previously established

crack. The splat radius was typically 0.5 cm. Using the value for fused quartz of $D = 9.5 \times 10^{-7}$ m²/s in Eq. (18) to predict the time at which the maximum tensile occurs, one finds $t^* = 1.7$ s. This value compares favorably with the first cracking event reported by Matthys. The second event is believed to be associated with the cooling phase of the bonded solidified splat mentioned above. The tensile stress levels induced by the splat from Eq. (18), on the other hand, appear to be too low to initiate cracking. Equivalently, the quartz substrate material appears to readily meet the condition (Eq. (14)) on temperature for the 1600°C splat. Thus, it remains to understand how the cracks are initiated in this particular experiment.

Coupling in the heat transfer problem between the splat and the substrate has not been considered here nor has the role of a thermal coating considered in Ref. 2. If the time at which cracking is predicted to occur, typically $tD/R^2 = 0.02$ to 0.1, is short compared to the time it takes the splat to undergo significant cooling, then the present results may be reasonably accurate without further modification. This might be the case, for example, for a splat medium undergoing solidification. The coupled problem should be considered if the splat temperature drops significantly prior to the predicted time of cracking or if for any reason the temperature at the surface of the solid varies rapidly with time after the first sudden increase.

APPENDIX

(1) Plane-Strain Cracking Problems

The problem of the subsurface crack oriented perpendicular to the free surface is solved using standard integral equation techniques. The geometry and the stress distribution of the uncracked half-space possess symmetry with respect to the crack line, so only opening displacements need be considered. The crack is represented by a dislocation distribution which is chosen to cancel the traction on the crack faces. The solution for a dislocation below the traction-free surface of the half-space is available in the literature, and the numerical procedure of Erdogan and Gupta[10] for solving the integral equation can be effectively used.

The problem of generating the trajectory of a very short crack initiated parallel to and below the surface when the crack is required to advance as a pure mode I crack has been treated in other contexts.[5–9] Given a smoothly curved subsurface crack, the solution can be produced using the same procedures as described in the previous paragraph, except that both tangential and opening displacements of the crack face must be considered. Because of the symmetry of the stress distribution with respect to the plane $x = 0$, only trajectories which were symmetric with respect to that plane were considered. Assuming that the crack at its current length has $K_{II} = 0$, then the crack length is increased with a change in curvature of the next increment chosen such that the advanced tip also is in a state of pure mode I. The procedure used here for incrementing the crack was identical to that used in Refs. 7 and 8.

(2) Axisymmetric Problems

As mentioned in the body of the paper, finite element methods were used to solve each of the three subproblems. Eight-noded isoparametric elements were used, and the same mesh is employed for the heat conduction problem as for the stresses induced in the uncracked half-space.

Equation (5) governs the evolving temperature change, $\Delta T(r,z,t)$. The following variational statement of Eq. (5) is used as the basis of the numerical solution to the transient problem:

$$D^{-1}\int_V \frac{\partial \Delta T}{\partial t}\delta T \, dV = -\int_V \vec{\nabla}\Delta T\cdot\vec{\nabla}\delta T \, dV + \int_S (\dot{n}\cdot\vec{\nabla}\Delta T)\delta T \, dS \tag{25}$$

where δT is the variation of T. A finite body was used in the numerical solution. It was taken to be a circular cylinder with outer radius $R_0 = 10R$ and height $H_0 = 10R$. Apart from the region $r \le R$ on the top surface, where ΔT is prescribed to be ΔT_0 for $t \ge 0$, the surface is everywhere taken to be perfectly insulated, assuming that negligible heat is lost from the unheated portion of the surface. The choices for R_0 and H_0 ensure that the zone of appreciable temperature increase is confined to a relatively small volume of the body and that the thermal stresses induced remain negligible in most of the volume analyzed. The stress–strain relations for the elastic material subject to a field of temperature increase ΔT relative to the initial uniform temperature are

$$\sigma_{ij} = L_{ijkl}(\varepsilon_{kl} - \alpha\Delta T\delta_{kl}) \tag{26}$$

At a given time t, the temperature field ΔT is known from the numerical solution of Eq. (25), and the corresponding stress fields and strain fields are found by a numerical solution based on using Eq. (26) in the principle of virtual work. At the bottom surface, $z = -10R$, far from the heated region, symmetry conditions have been prescribed with $u_z = 0$ and zero shear tractions. All the other surfaces are taken to be traction-free.

As mentioned in the body of the paper, the crack is imagined to develop in the uncracked half-space at a given time t with its associated temperature and stress distribution. In other words, the crack is assumed to grow after the temperature and stress distributions in the uncracked body have been established. The growth process is likely to be dynamic, and any subsequent influence of the crack on the temperature distribution has not been considered.

In each crack analysis, the energy release rate G is determined by the stiffness derivative finite-element technique,[11] which involves derivatives with respect to crack advance for element stiffness and load terms resulting from thermal expansion. The computations are still based on the principle of virtual work with Eq. (26) substituted for the thermoelastic behavior, but the mesh is highly refined near the crack tip, with several rings of small elements around the tip. The J-integral is used to evaluate the energy release rate, using the actual strain energy density expansion accounting for thermal expansion.[12] For these axisymmetric crack problems, the J-integral values obtained on contours of very small radius around the tip agree with the values obtained by the stiffness derivative technique within 2%–4%. The ratio of the stress intensity factors, K_{II}/K_I, is needed to evaluate ψ in Eq. (22). Approximate values of the stress intensity factors were obtained by substituting stress values at two integration points symmetrically placed about the crack plane into the well-known analytical expressions for the singular near-tip fields. Corresponding values of the energy release rate evaluated using the K's obtained in this manner in Eq. (21) differ by from 5% to 15% from the accurate values obtained from the methods mentioned above. Thus, the magnitudes of the values of K_I and K_{II} obtained from the singular fields are not very accurate, but it is assumed that the ratio of their values in Eq. (22) should give a reasonable representation of mode mixity.

Finally, it is noted again that the assumption of traction-free surfaces used in the present studies excludes the type of spalling mentioned in the Conclusions, where a hot splat solidifies, bonds to the substrate, and then drives a crack through surface tractions upon cooling.

References

[1]D. Backman, "Metal-Matrix Composites and IPM: A Modeling Perspective," *J. Met.*, July, 17–20 (1990).

[2]E. S. Russell, "Model for Fiber Thermal Shock during Plasma Spray Deposition," Rep. No. R90AEB1039, Technical Information Series, GE Aircraft Engines, Lynn, MA, Oct. 1990.

[3]W. Jaunzemis and E. Sternberg, "Transient Thermal Stresses in a Semi-infinite Slab," *J. Appl. Mech.*, **27**, 93–103 (1960).

[4]A. Jahanshahi, "Transient Stresses Induced by Heating a Plane Boundary," *Int. J. Solids Struct.*, **9**, 1–14 (1973).

[5]P. A. Wawrzynek and A. R. Ingraffea, "Interactive Finite Element Analysis of Fracture Processes: An Integrated Approach," *Theor. Appl. Mech.*, **8,** 137–50 (1987).

[6]D. V. Swenson and N. Kaushik, "Finite Element Analysis of Edge Cracking in Plates," *Eng. Fract. Mech.*, **37,** 641–52 (1990).

[7]N. A. Fleck, "Brittle Fracture due to an Array of Microcracks," *Proc. R. Soc. London, A*, **432,** 55–76 (1991).

[8]L. B. Freund and K. S. Kim, "Spiral Cracking around a Strained Cylindrical Inclusion in a Brittle Material and Implications for Vias in Integrated Circuits"; in the proceedings of the 1991 MRS Spring Meeting, Anaheim, CA in Symposium H: Mechanical Behavior of Materials and Structures in Microelectronics, 1991. Materials Research Society, Pittsburgh, PA, 1991.

[9]J. W. Hutchinson and Z. Suo, "Mixed Mode Cracking in Layered Materials"; pp. 64–187 in *Advances in Applied Mechanics,* Vol. 29. Edited by J. W. Hutchinson and T. Y. Wu. Academic Press, New York, 1991.

[10]F. Erdogan and G. D. Gupta, "On the Numerical Solution of Singular Integral Equations," *Q. Appl. Math.*, **30,** 525–34 (1972).

[11]D. M. Parks, "A Stiffness Derivative Finite Element Technique for Determination of Crack Tip Stress Intensity Factors," *Int. J. Fract.*, **10,** 487–502 (1974).

[12]C. F. Shih, B. Moran, and T. Nakamura, "Energy Release Rate along a Three-Dimensional Crack Front in a Thermally Stressed Body," *Int. J. Fract.*, **30,** 79–102 (1986). □